Supplementary Information (SI) for Energy & Environmental Science.
This journal is © The Royal Society of Chemistry 2025

Supplementary Information

Charge carrier management for highly efficient perovskite/Si tandem solar cells with poly-Si based passivating contacts

Xuzheng Liu,[ab] Michael Rienaecker,[cd] Mohammad Gholipoor,[ab] Lingyi Fang,[ab] Tonghan Zhao,[a] Benjamin Hacene,[b] Julian Petermann,[ab] Ruijun Cai,[b] Hang Hu,[ab] Thomas Feeney,[b] Faranak Sadegh,[ab] Paul Fassl,[ab] Renjun Guo,[*ab] Uli Lemmer,[ab] Robby Peibst,[*cd] and Ulrich Wilhelm Paetzold[*ab]

[*] Corresponding authors

[a] Institute of Microstructure Technology (IMT), Karlsruhe Institute of Technology (KIT), Hermann-von-Helmholtz-Platz 1, 76344, Eggenstein-Leopoldshafen, Germany

[b] Light Technology Institute (LTI), Karlsruhe Institute of Technology (KIT), Engesserstrasse 13, 76131, Karlsruhe, Germany

[c] Institute for Electronic Materials and Devices, Leibniz University Hannover, Schneiderberg 32, 30167, Hannover, Germany

[d] Institute for Solar Energy Research Hamelin (ISFH), Am Ohrberg 1, 31860, Emmerthal, Germany

*Email: ulrich.paetzold@kit.edu, peibst@isfh.de, renjun.guo@kit.edu

Materials and Methods

Materials

Dimethyl sulfoxide anhydrous ≥99.9% (DMSO, CAS: 67-68-5), N, N-dimethylformamide ≥99.9% (DMF, CAS: 68-12-2), and Ethyl Acetate anhydrous 99.8% (EA, CAS: 141-78-6) were purchased from Sigma Aldrich. Formamidinium iodide (FAI, CAS: 879643-71-7), Methylammonium Bromide (MABr, CAS: 6876-37-5), Propane-1,3-diammonium iodide ($PDAI_2$, CAS: 120675-53-8), n-Butylammonium iodide (BAI, CAS: 36945-08-1) was bought from Greatcell Solar. Lead iodide (PbI_2, CAS: 10101-63-0) and Lead Bromide ($PbBr_2$, CAS: 10031-22-8), Cesium Iodide (CsI, CAS: 7789-17-5) was purchased from VWR. Fullerene-C_{60} (C_{60}, CAS: 99685-96-8) was purchased from Sigma-Aldrich. 2PACz (CAS: 20999-38-6) were synthesized by TCI. Isopropanol 99.8% and Ethanol absolute 99.8% was bought from VWR Chemicals. All the materials were used as received without any purification.

Perovskite precursor solutions

The 1.68eV triple-cation perovskite absorber solution $Cs_{0.05}(FA_{0.77}MA_{0.23})_{0.95}Pb(I_{0.77}Br_{0.23})_3$ was prepared with the precursors methylammonium bromide (MABr), formamidinium iodide (FAI), lead iodide (PbI_2), lead bromide ($PbBr_2$), and cesium iodide (CsI, 7789-17-5, Alfa Aesar). Two solutions were prepared: 1) FAI (191mg), PbI_2 (558.3mg), MABr (38.1mg), and $PbBr_2$ (136.5mg) in 800µl *N*, *N*-dimethylformamide (DMF, 68-12-2, Sigma Aldrich) and 200µl dimethyl sulfoxide (DMSO, 67-68-5, Sigma Aldrich) with the volume ratio of 4:1 and 2) CsI (390mg) in 1ml DMSO. Adding 50 µL of solution 2) into solution 1) to get the final triple cation perovskite solution.

Methods

Single-junction wide bandgap perovskite solar cell

The indium tin oxide (ITO) glass substrates are cleaned by ultra-sonication in acetone and isopropanol for 15 min each. For the hole transport layer (HTL), a 1.63 mmol/l 2PACz solution in ethanol is spin-coated at 3000 rpm for 30 sec and annealed at 100°C for 10 min in N_2 atmosphere. The 1.5M 1.68eV triple-cation perovskite absorber solution $Cs_{0.05}(FA_{0.77}MA_{0.23})_{0.95}Pb(I_{0.77}Br_{0.23})_3$ was spin-coated onto

the hole transport layer by two following steps: 1) 1000 rpm rotation speed for 10 s and 2) 5000 rpm for 30 sec, with 2000 rpm s^{-1} acceleration rate. After 17-20 sec of second step, 150µl ethyl acetate (EA), was dynamically released as anti-solvent on the spinning substrate. Samples were annealed at 100°C for 30min in N_2 atmosphere. A solution of 0.3 mg/ml $PDAI_2$ and 0.3mg/ml BAI is spin-coated at 4500 rpm for 30 sec and annealed at 100°C for 5min in N_2 glovebox. For the electron transport layer (ETL), 20nm C_{60} was thermally evaporated on the perovskite films under a high vacuum of lower than 10^{-6} Tor, followed by 5nm BCP evaporation as a hole-blocking layer. Finally, 100nm Ag electrode was evaporated under a high vacuum of lower than 10^{-6} Tor.

Silicon bottom cell with POLO contacts

A thin SiOx layer is thermally grown on a double-side chemically mechanically polished 275-µm-thick n-type wafer with a resistivity of 3.3 Ω cm. We subsequently cap the interfacial oxide by a low-pressure chemical vapor deposited (LPCVD) intrinsic amorphous Si layer. We perform Phosphorus and Boron implantation to dope the a-Si on the front and rear sides, respectively. Then, the amorphous Si recrystallizes during wet oxidation to grow a thick SiO_2 layer and the POLO junctions form in a subsequent higher temperature process at 1035°C yielding electron- and hole-selective passivating polysilicon-on-passivating-oxide (n-POLO and p-POLO) contacts. On the rear side, laser ablation is used to pattern the SiO_X so that only isolated p-POLO contact islands remain after KOH etching and texturization. During the latter processing step, the SiO_X protects the front-side n-POLO contact and the rear-side p-POLO islands. Then the front-side SiO_X is removed via single-sided HF treatment, and the poly-Si thickness is reduced to ~50 nm using an isotropic etch in an ammonium-peroxide mixture.

After stripping the SiO_X from the rear side, the rear side is passivated with a stack of aluminum oxide (Al_2O_3), silicon nitride (SiN_y), and SiO_X, while the front receives an Al_2O_3 layer to facilitate hydrogenation of the n-POLO contact. The dielectric stack on the rear is then selectively ablated on the p-POLO islands to allow for electrical contact with the metal. Next, the cell precursor undergoes a diluted HF dip to remove the Al_2O_3 hydrogenation layer from the front side. An indium tin oxide (ITO) layer is sputtered onto the front n-POLO contact to form a transparent conductive electrode. The ITO

layer was sputtered using a 90/10 In_2O_3/SnO_X target (90 wt% indium oxide, 10 wt% tin oxide), with a purity of 99.99%. To minimize parasitic absorption in the front-side ITO layer, we use a bilayered ITO structure, consisting of a 3 nm seed ITO layer sputtered without O_2 flow, resulting in a high carrier density to ensure proper contact formation with the poly-Si, followed by a 10 nm transparent ITO top layer reactively sputtered with O_2. After the ITO deposition, SiO_X isolation strips are sputtered onto the front side and annealed in a vacuum at ~ 350°C. Finally, a rear-sided HF treatment is performed before evaporating the aluminum (Al) back contact into the cell area through a $12\times12mm^2$ mask onto the rear side. The wafers are laser scribed on the rear side and cleaved into 25×25 mm² substrates, yielding 1 cm² solar cells.

This design builds upon our prior advancements in polycrystalline silicon (poly-Si)-based passivating contacts, integrating them in a novel manner to optimize carrier selectivity and minimize recombination losses.[1, 2] Our approach leverages the exceptional charge carrier selectivity of passivating polysilicon on oxide (POLO) junctions, which exhibit record-low minority carrier recombination current density (J_0) and ultra-low junction resistivity. These characteristics enable "perfect contacts" with selectivity values exceeding S_{10} >16 for both polarities - with alkaline surface texturing to ensure sufficient light trapping in the bottom cell.[3] Furthermore, we incorporated an alkaline surface texturing process to enhance light trapping and maximize the bottom cell's photocurrent generation. This combination of superior carrier selectivity and effective light management ensures the silicon bottom cell achieves optimal electrical and optical performance, forming a robust foundation for the tandem architecture.[2]

Tandem solar cell

The bottom silicon substrates were spin coated by acetone and isopropanol as washing steps, and then annealed at 300°C for 10min in N_2 to activate the silicon substrates. The annealed silicon bottom cells were treated by oxygen plasma for 30 sec before NiO_X deposition. 5, 15, 25-nm NiO_X layers were deposited onto an ITO substrate via sputtering from a NiO_X target, using 100 W power in a pure Ar atmosphere at a pressure of 1 mTorr. The same SAM, perovskite, $PDAI_2$ and BAI, 15nm C_{60} deposition as described above was conducted on the substrates. A 20 nm SnO_X buffer layer was fabricated using

atomic layer deposition (ALD) at a substrate temperature of 90°C. Tetrakis(dimethylamino)tin (IV) (TDMASn) was used as the precursor source at 70°C, while H_2O served as the reactant, held at 18°C. For TDMASn, the pulse and purge times were 1.6 s and 12.0 s, respectively, with a 120 sccm N_2 flow. For H_2O, the pulse and purge times were 0.1 s and 16.0 s, respectively, with a 150 sccm N_2 flow. A total of 200 ALD cycles were performed. Then, 35 nm indium zinc oxide (IZO) was deposited by sputtering using a 190W power with Ar and O_2 at 1mTorr, as the top transparency conductive oxide (TCO). After that, the silver electrode with grid fingers of 600 nm was thermally evaporated as the top contact. Finally, 100 nm magnesium fluoride (MgF_2) was evaporated on as an anti-reflective coating (ARC) for better light management.

Solar Cell Characterizations

Current density voltage (*J-V*) characteristics

Single-junction perovskite solar cell. The *J-V* characteristics of the perovskite solar cells (PSCs) were measured using a class AAA xenon-lamp solar simulator (Newport Oriel Sol3A) and a Keithley 2400 source meter under an air-mass 1.5 global (AM1.5G) spectrum at an illumination intensity of 100 mW cm^{-2}. The solar simulator's irradiation intensity was calibrated using a scan rate of 0.6 V s^{-1} and a certified silicon solar cell (Fraunhofer ISE CalLab) equipped with a KG5 bandpass filter. Stabilized power conversion efficiency (PCE) was determined by measuring the photocurrent at the maximum power point (MPP) using a perturb-and-observe algorithm under continuous AM1.5G illumination. During all measurements, the devices were maintained at a temperature of 25°C using a Peltier element controlled by a microcontroller. The single-junction PSCs has an active area of 10.5 mm^2, and the *J-V* measurements were conducted in a nitrogen-filled glove box.

Tandem solar cell. The J−V characteristics of the perovskite-silicon tandem solar cells (PSTSCs) were measured using an LED-based solar simulator (WaveLabs Sinus 70) and a Keithley 2400 source meter under an air-mass 1.5 global (AM1.5G) spectrum at an illumination intensity of 100 mW cm^{-2}. The

irradiation intensity of the solar simulator was calibrated using a certified silicon solar cell (Fraunhofer ISE CalLab). The active area was defined by a shadow mask with an aperture area of 1.0 cm^2. The devices were tested using both reverse scans (2 V to -0.2 V, 20 mV steps) and forward scans (-0.2 V to 2 V, 20 mV steps) at a scan rate of 10 mV s^{-1}. The J−V measurements were conducted at room temperature in ambient condition. The maximum power point (MPP) tracking of tandem devices without any encapsulation was conducted under ambient air using 1 Sun LED illumination (WaveLabs Sinus 220) at a controlled temperature of 25°C.

External Quantum Efficiency (EQE)

Single-junction perovskite solar cell. The external quantum efficiency (EQE) spectra of the perovskite solar cells (PSCs) were measured using a Bentham PVE300 system with modulated monochromatic light. The chopping frequency was set to 570-590 Hz. The spectra were acquired over a wavelength range of 300 to 850 nm using a chopping frequency of 560–590 Hz and an integration time of 500 ms. The EQE measurements were performed in a nitrogen-filled glovebox.

Tandem solar cell. The equipment, chopping frequency and integration time for EQE measurements of the perovskite-silicon tandem solar cells (PSTSCs) were the same as those used for the single-junction PSCs mentioned above. The spectra were acquired over a wavelength range of 300 to 1200 nm calibrated by the certified silicon (Si) and germanium (Ge) reference cells for the wavelength ranges of 300–1100 nm and 1000–1300 nm, respectively. The EQE measurements for each sub-cell were conducted using a combination of bias light sources to saturate the other sub-cell completely. For the perovskite top cell, IR LED light sources at 780 nm and 940 nm were used. For the silicon bottom cell, a blue LED light sources at 465 nm and a white LED were used. The EQE measurements were also performed in a nitrogen-filled glovebox.

Long term stability measurements

The long-term operational stability of unencapsulated devices was evaluated using a solar cell stability test system under ambient air conditions, with a controlled relative humidity of approximately 30-40%. The testing system employed a white light-emitting diode (LED) lamp (Puri Materials) as the

illumination source, delivering a power density of 100 mW cm^{-2}. The device temperature was maintained at 25°C throughout the testing period to ensure environmental stability.

Estimation of T_{80} Lifetime

The operational stability of the perovskite solar cell was analyzed using an exponential decay model to estimate its T_{80} lifetimes. Given that the device retained 93% of its initial efficiency after 240 hours under MPPT operation, we assumed an exponential efficiency degradation, expressed as:

$$\eta(t) = \eta_0 \cdot e^{-\lambda t}$$

where $\eta(t)$ is the efficiency at time t, η_0 is the initial efficiency (normalized to 1), and λ is the decay constant.

Silicon Characterizations

Calculation of implied recombination current density J_{rec} and implied open -circuit voltage iV_{OC} from Infrared Lifetime Mapping (ILM) Method

The Infrared Lifetime Mapping (ILM) method is a calibration-free technique for dynamically mapping the carrier lifetime in silicon samples. It measures the infrared emission of free charge carriers that occurs after illumination with monochromatic light. By comparing signals immediately after illumination and in steady-state conditions, the effective carrier lifetime τ_{eff} can be determined. This method enables fast, spatially resolved analysis. Further details on the ILM technique can be found in Ref.[4]

Determining the Recombination Current Density J_{rec}

The recombination current density J_{rec} is calculated from the generation current density based on the measured photon flux Φ_{ph} under 1 sun illumination, the elementary charge q, the illumination intensity I in Suns, and the reflectance R of the sample. Since, under steady-state conditions, generation and recombination are balanced, J_{rec} is given by:

$$J_{rec} = q \cdot (1 - R) \cdot \Phi \cdot I$$

Calculating the Excess Carrier Density Δn

The excess carrier density Δn is determined using the relationship between J_{rec} and the effective carrier lifetime τ_{eff} :

$$\Delta \mathrm{n} = \frac{J_{rec}}{q \cdot W \cdot \tau_{eff}}$$

where W is the sample thickness.

Calculating the Implied Open-Circuit Voltage iV_{OC}

The implied open-circuit voltage iV_{OC} is derived from the pn product with the excess carrier density Δn, the equilibrium carrier densities n_0 and p_0 for electrons and holes by using:

$$\mathrm{i}V_{OC} = \frac{kT}{q} \ln \left(\frac{(\Delta \mathrm{n} + \mathrm{n}_0) \cdot (\Delta \mathrm{n} + \mathrm{p}_0)}{{n_i}^2}\right)$$

where k is the Boltzmann constant, T is the temperature in Kelvin, and n_i is the intrinsic carrier concentration of silicon.

Calculating the pseudo current density-voltage characteristic

By measuring under different illumination intensities, a J_{rec}-iV_{OC} characteristic can be obtained, providing insight into the recombination behavior of the silicon solar cell. When assuming a short-circuit current density J_{SC} for the silicon solar cell, we can derive a current density-voltage characteristic to find an iV_{OC} and FF at the assumed J_{SC} at (filtered) 1sun conditions.

Thin Film Characterizations

Time-correlated single photon counting (TCSPC)

TCSPC measurements were performed with a FLS920 fluorescence spectrometer (Edinburgh Instruments Ltd 2006) and a 635 nm laser (LDH-P-635, Pico Quant) at a 50 kHz repetition rate. The laser power density is 4.33 nJ cm^{-2}.

We utilize the mono exponential model to fit the decay curve according to the equation below, [5]

$$y = \sum_i A_i e^{-x/\tau_i}$$

Where i = 1 corresponding to mono-exponential fitting.

PLQY

PLQY measurements were performed in a nitrogen-flushed integrating sphere (LabSphere, 15 cm diameter, relative humidity <5%). A green laser (LD-515-10MG, Roithner Lasertechnik) was directed into the sphere through a small entrance port. Emission from the sphere's exit port was collected using an optical fiber and analyzed by spectrometers (QEPro, Ocean Optics). The spectral response was calibrated with a calibration lamp (HL-3plus-INT-Cal, Ocean Optics), and the raw spectra were converted to power spectra based on the integration time. The PLQY was calculated following the method outlined by de Mello et al.[6] To minimize specular reflectance, samples were positioned at a 15° angle relative to the laser beam. The implied VOC was derived from intensity-dependent PLQY measurements as described by Stolterfoht et al.[7] and Kirchartz et al.[8] The ideality factor and parameters from pseudo-*JV* were obtained from the light intensity dependent PLQY measurements.

PL Intensity maps

Two 467 nm LED bars, aligned opposite at 45° to the image plane, illuminate the sample to provide a homogenous excitation equivalent to 0.2 suns. The resulting photoluminescence is imaged by a sCMOS camera equipped with a macro zoom lens and a 695 nm absorptive long-pass filter. The resulting images are measured with an exposure time of 50 ms and are background corrected for stray light and camera noise.

X-ray diffraction (XRD)

X-ray diffraction (XRD) measurements were performed on samples of POLO-Si/ITO using a Bruker D2 Phaser diffractometer equipped with a LynxEye detector. The measurements employed Cu Kα radiation (λ = 1.5405 Å) in the Bragg-Brentano geometry.

Scanning electron microscope (SEM)

The top-view scanning electron microscopy (SEM) images were acquired using a Zeiss LEO 1530 VP microscope equipped with an in-lens detector.

Atomic force microscopy (AFM)

The surface topographies of the substrates deposited with ITO layer (0, 5, 20nm) and NiO_X (0, 5, 15, 25nm) were measured using a Nano Wizard II (JPK Instruments) atomic force microscope, with a scanning area of 10 μm × 10 μm.

Specific surface area (SSA)

The specific surface area (SSA) of the thin film is determined based on 3D atomic force microscopy (AFM) morphology data and then computed using the following formula:

$$SSA = \frac{A_S}{V_{total}}$$

Where A_S is the real surface area of the thin film,

V_{total} is the total volume of the protrusions on the rough surface of the thin film, approximated as a series of conical structures.

To determine the real surface area (A_S) of the thin film, 3D AFM data containing 512×512 pixels with x, y, z coordinates is analyzed. The real surface area is calculated by discretizing the AFM height map into small triangular facets and summing their individual surface areas. By summing the areas of all triangular elements, the total real surface area (A_S) is obtained:

$$A_S = \sum_{i=0}^{n} A_{triangle,i}$$

Where N is the total number of triangles in the structured map based on AFM data.

To quantify the total volume of surface protrusions on the rough thin film, the protrusions are approximated as tiny truncated cones (frustums) and full cones, depending on their geometry. The baseline height determined as the median surface level, and all protrusions exceeding a predefined height threshold are segmented for volume estimation. The total volume is obtained by summing the individual volumes of all identified structures:

$$V_{total} = \sum_{i=1}^{N} V_i$$

Where N is the number of detected truncated cones or cones.

Simulation of Minority Carrier Lifetime: Impact on Solar Cell Efficiency

This simulation process used to investigate the impact of electron (τ_n) and hole (τ_p) minority carrier lifetimes on the efficiency of silicon solar cells. The simulation aims to visualize the dependence of solar cell efficiency on carrier recombination properties, which is crucial for optimizing device performance.

Simulation Methodology. The efficiency of a silicon solar cell is primarily determined by the short-circuit current density (J_{SC}), open-circuit voltage (V_{OC}), and fill factor (FF), which are functions of minority carrier lifetimes. The parameters are derived based on the following equations,

$$L_n = \sqrt{D_n * \tau_n}\ , L_p = \sqrt{D_p * \tau_p}$$

$$J_0 = \frac{(q * {n_i}^2)}{N_d * \tau} * \exp\left(-\frac{E_g}{kT}\right)$$

$$V_{OC} = \left(\frac{kT}{q}\right) * \ln\left(\frac{J_{ph}}{J_0} + 1\right)$$

$$FF = \frac{V_{OC} - \ln\left(V_{OC} + 0.72\right)}{V_{OC} + 1}$$

$$\eta = V_{OC} * J_{SC} * FF$$

Detailed parameters are illustrated in Table S2 and are extracted from the literature.

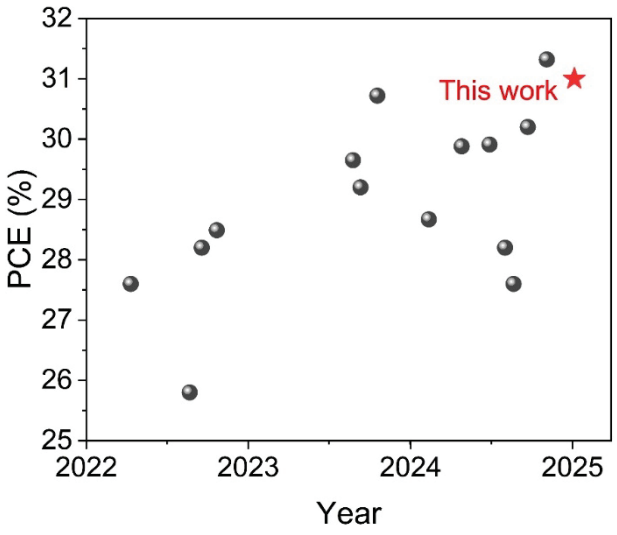

Figure S1. PCE statistics of published perovskite/Si tandem solar cells with poly-Si based passivating contacts in recent years.[9-21]

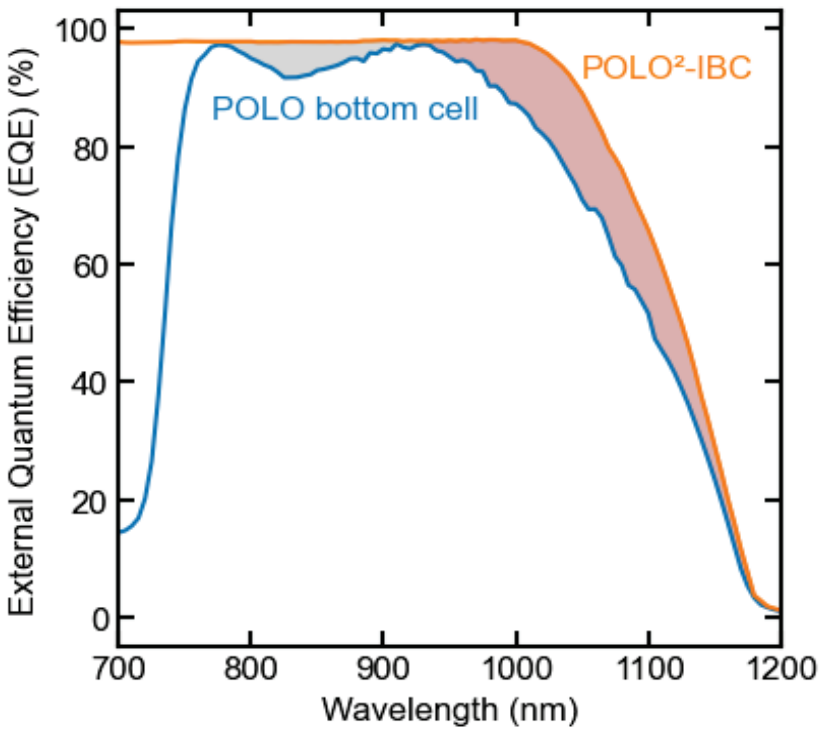

Figure S2. External quantum efficiency of the bottom solar cell in the Perovskite/Si tandem compared to a 26%-efficient POLO²-IBC single junction cell.

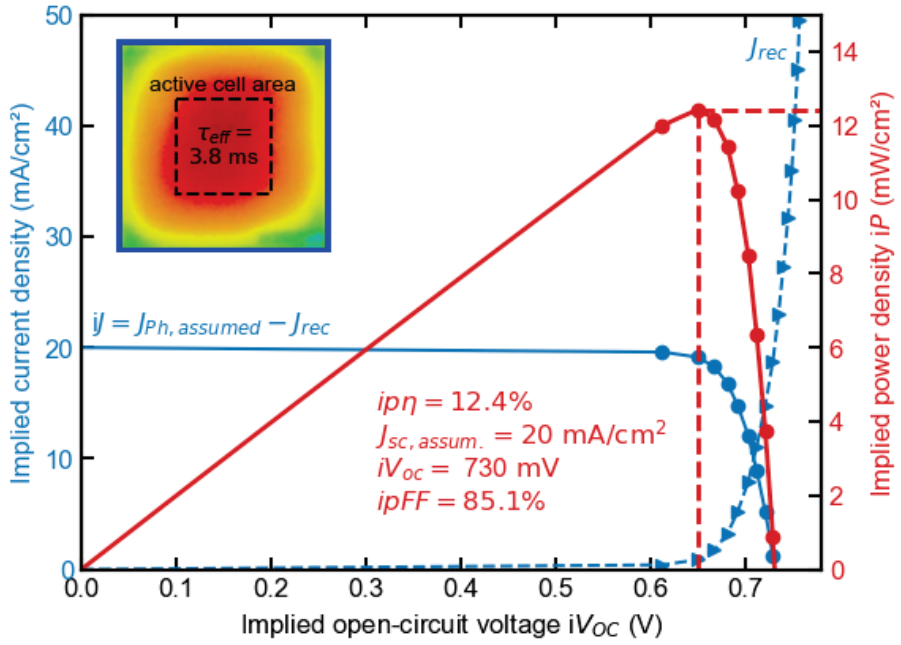

Figure S3. Implied current-voltage (iJ-iV_{OC}) and implied power density-voltage characteristics of the bottom solar cell as shown in (a), assuming a photogeneration current density J_{ph} of 20 mA·cm^{-2}. The implied current iJ was calculated from J_{rec}, derived from injection-dependent lifetime characteristics based on the infrared lifetime mapping method. The inset shows a lifetime image at an injection level of 6.7×10^{15} cm^{-3}, corresponding to an implied V_{OC} of 702 mV, with an effective carrier lifetime τ_{eff} of 3.8 ms in the active cell area.

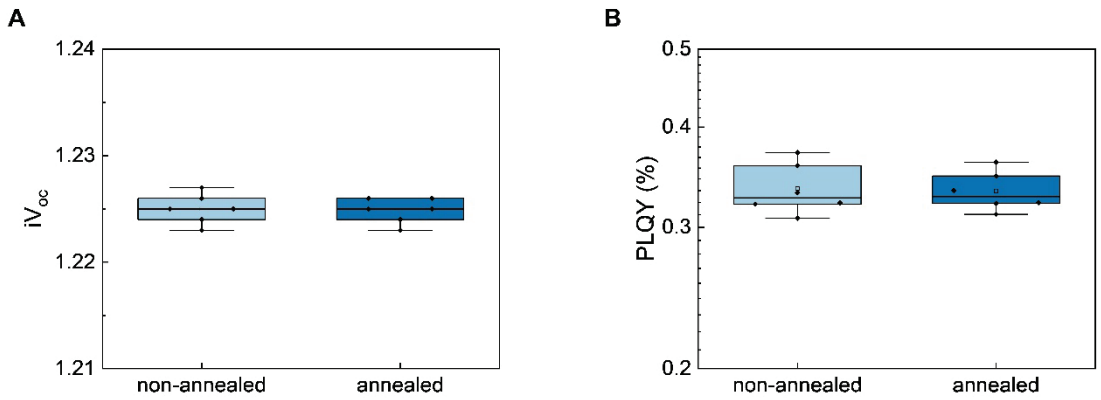

Figure S4. (A) iV_{OC} and (B) PLQY measurements of perovskite film performed on half stack samples (Si/ITO/NiO_X/2PACz/Perovskite) w.o. and w. annealing treatment.

Table S1. The implied open-circuit voltage (iVoc) and pseudo-fill factor (pseudo-FF) derived from the pseudo-*JV* curves.

	$J_{SC,assumed}$	*iVoc*	*ipFF*	iPCE
Before ITO sputtering	20	0.728	0.8497	12.38
After ITO sputtering	20	0.7	0.832	11.65
After ITO sputtering +annealing at 300°C	20	0.7346	0.8476	12.453

Table S2. The parameters for simulation of minority carrier lifetime impact on solar cell efficiency.

Description	Parameters
Temperature	300K
Intrinsic carrier concentration	1.5×10^{10} cm^{-3}
Diffusion coefficients	$D_n = 36$ cm^2/s, $D_p = 12$ cm^2/s
Photogenerated current density	40 mA cm^{-2}
Electron lifetime	10^{-12} s to 10^{-2} s
Hole lifetime	10^{-12} s to 10^{-2} s
SQ Limit efficiency	33.7%

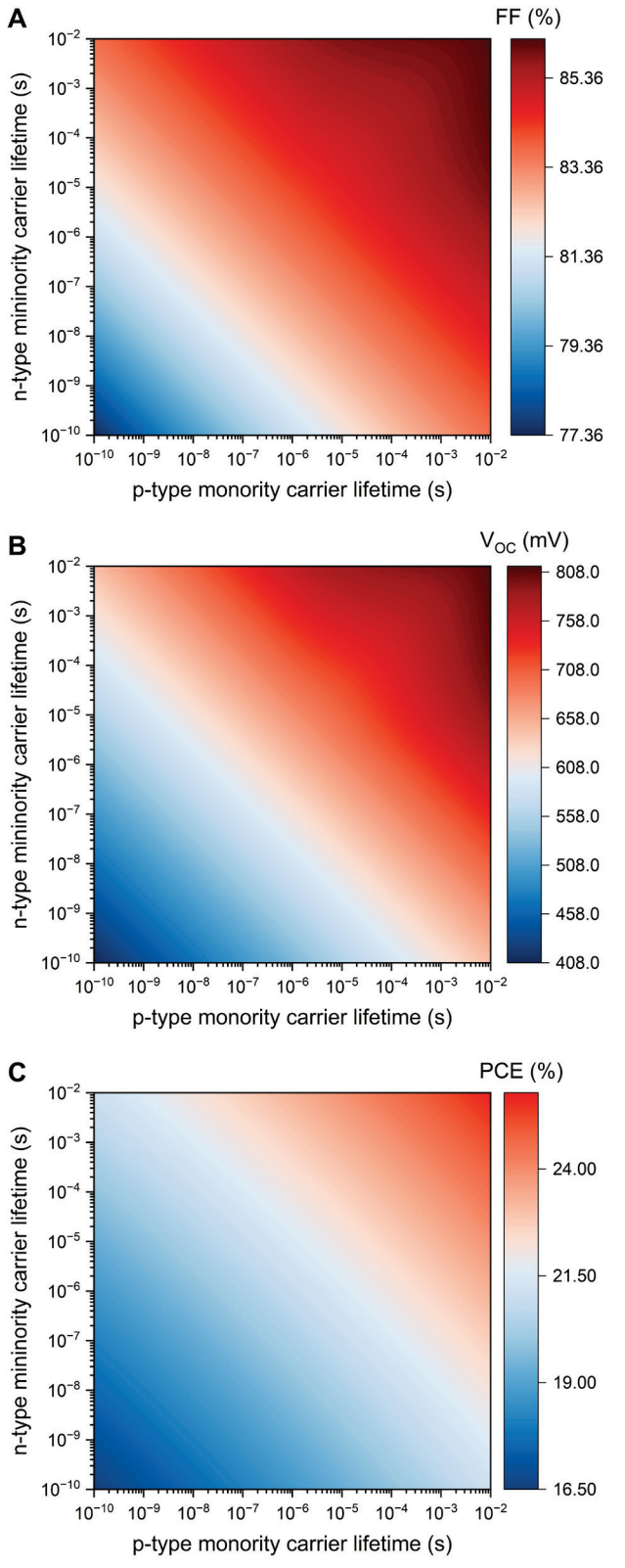

Figure S5. Numerical simulation illustrating how minority carrier lifetime effects Si solar cell's (A) *FF*, (B) V_{OC}, (C) PCE. This simulation quantitatively explains the correlation between lifetime improvement and enhanced device characteristics, providing theoretical support for the experimental findings.

Table S3. The square resistance of ITO layer on the Si bottom cell before and after N_2 annealing measured by four-point probe method.

	ITO before N_2 annealing	ITO after N_2 annealing
Square resistance (Ω/□)	114.8	91.3

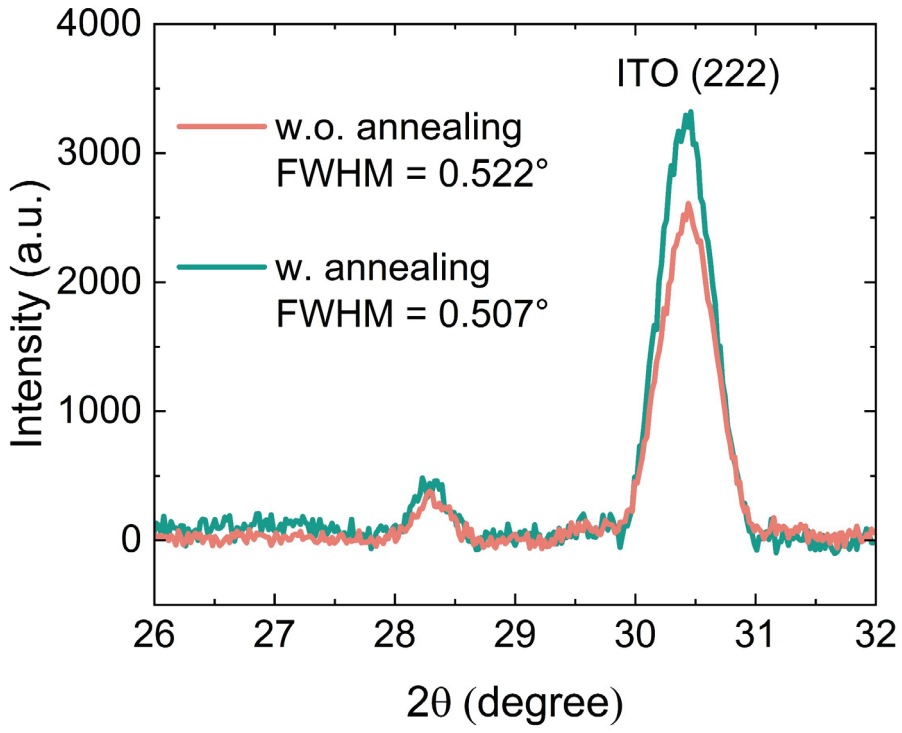

Figure S6. X-ray diffraction image of ITO thin films without and with annealing.

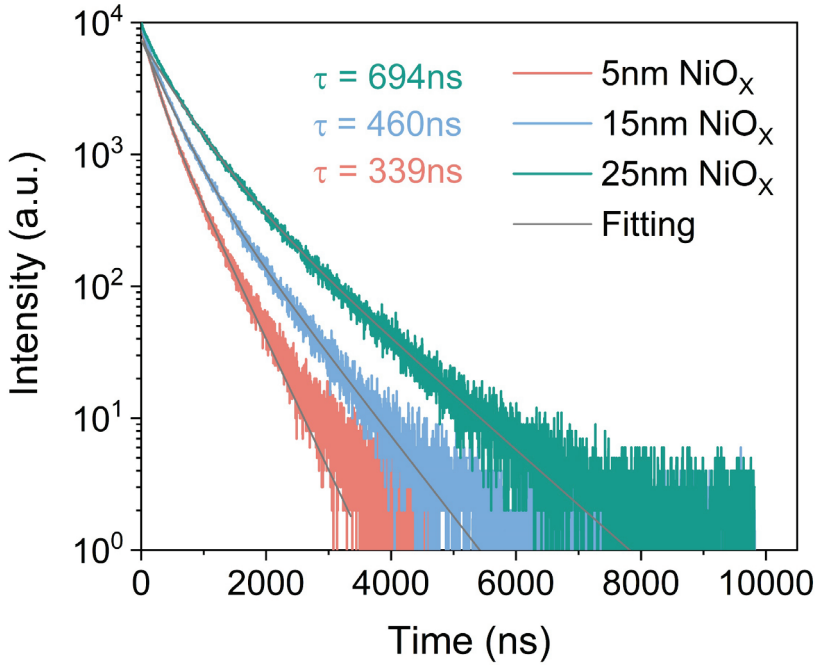

Figure S7. TRPL measurements performed on half stack samples (Si/ITO/NiO_X/2PACz/Perovskite) with different NiO_X thicknesses (5nm, 15nm and 25nm).

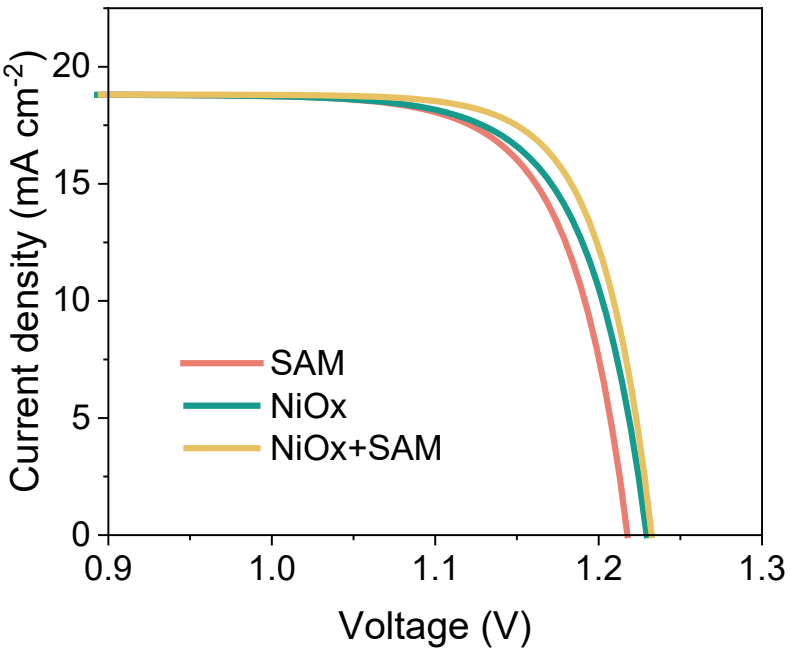

Figure S8. Pseudo-*JV* curves obtained from light intensity dependent iV_{OC} measurements on the Si/ITO/HTL/Perovskite with SAM alone, NiO_X alone, and NiOx+SAM.

Table S4. The implied open-circuit voltage (iVoc) and pseudo-fill factor (pseudo-FF) derived from the pseudo-*JV* curves.

	iVoc	*ipFF*
SAM	1.218	85.0
NiOx	1.229	84.2
NiOx+SAM	1.233	86.6

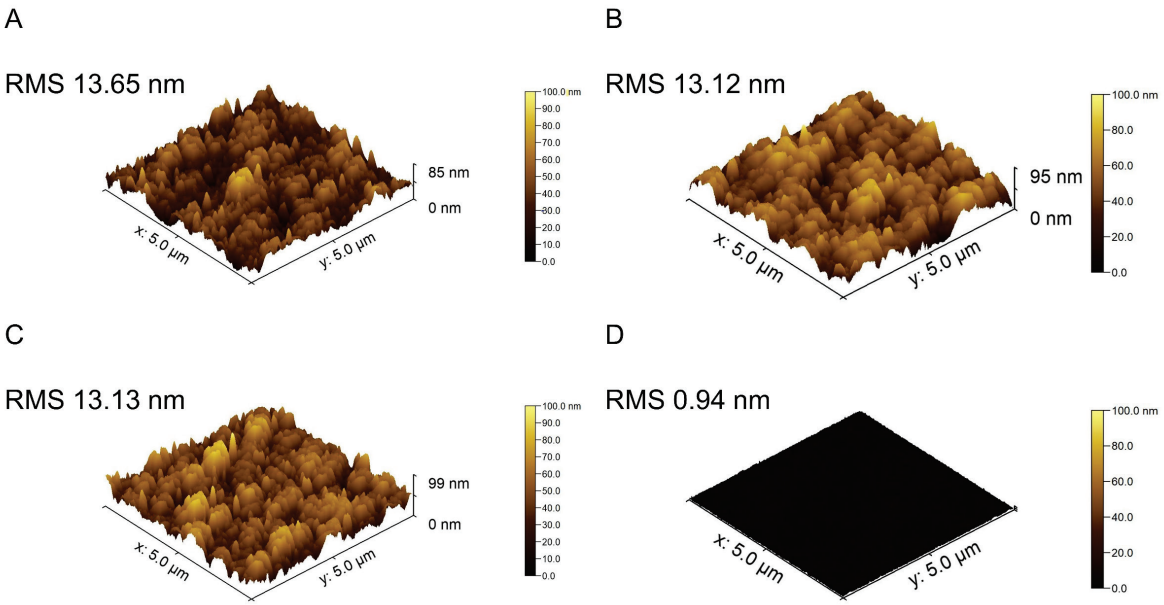

Figure S9. The 3D atomic force microscopy (AFM) images (5×5µm) of (A) 0nm ITO layer on the Si bottom cell, (B) 5nm ITO layer on the Si bottom cell, (C) 20nm ITO layer on the Si bottom cell, (D) 20nm ITO layer on the glass.

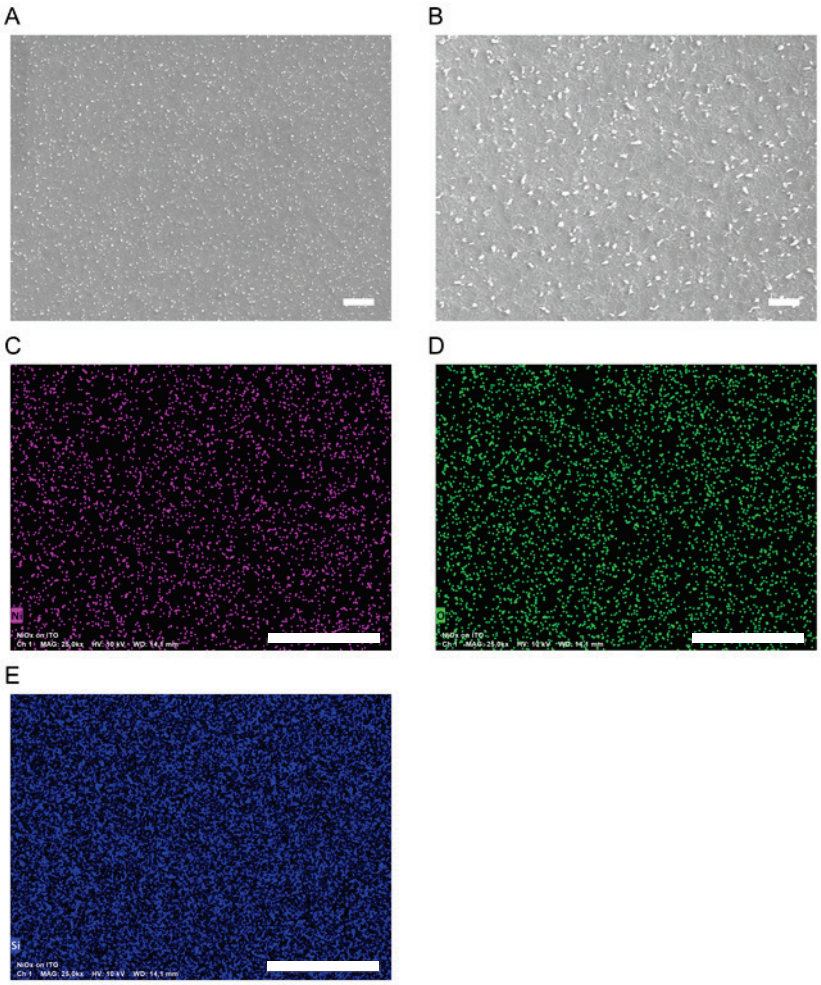

Figure S10. The SEM image of the Si bottom cell with an ITO layer after 5 nm NiO_X deposition by sputtering, (A) scale bar:1um, (B) scale bar:300nm. The corresponding EDX maps, (C) nickel, (D) oxygen, (E) silicon, scale bar: 1μm.

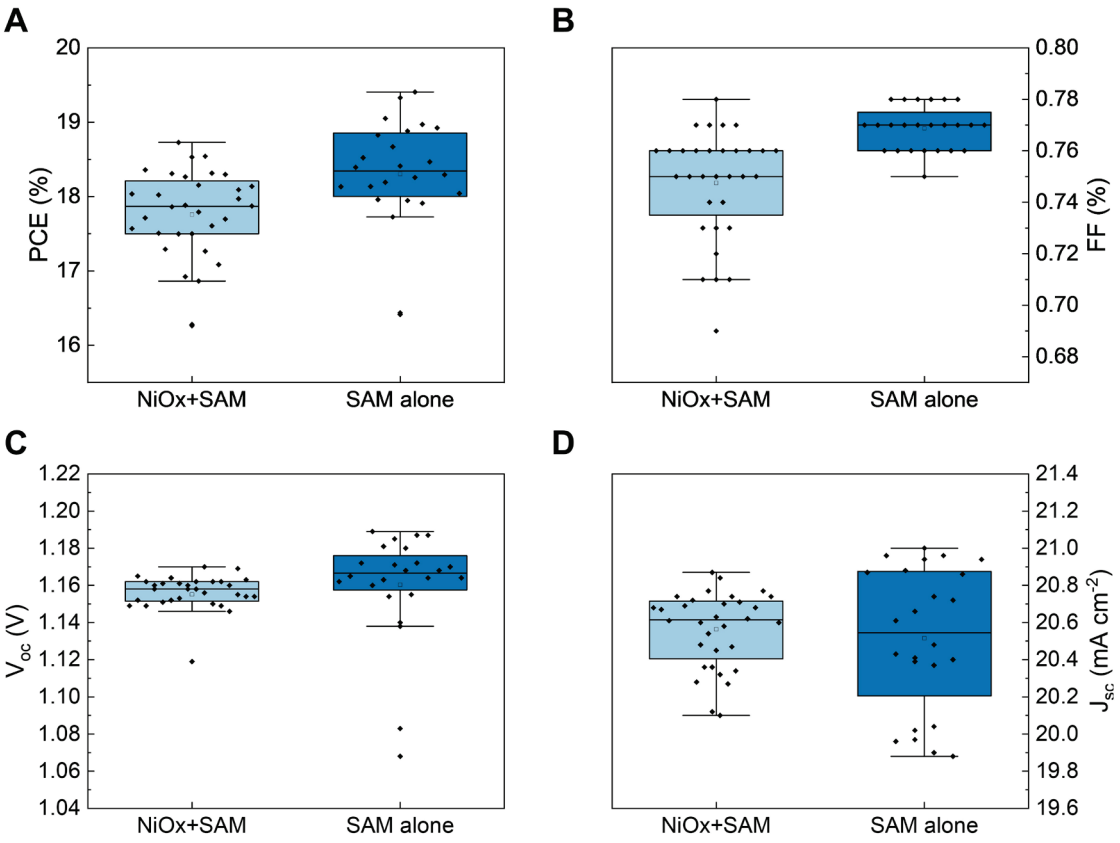

Figure S11. Statistical comparison of single junction perovskite solar cells performance with NiO_X+SAM or SAM alone as HTL.

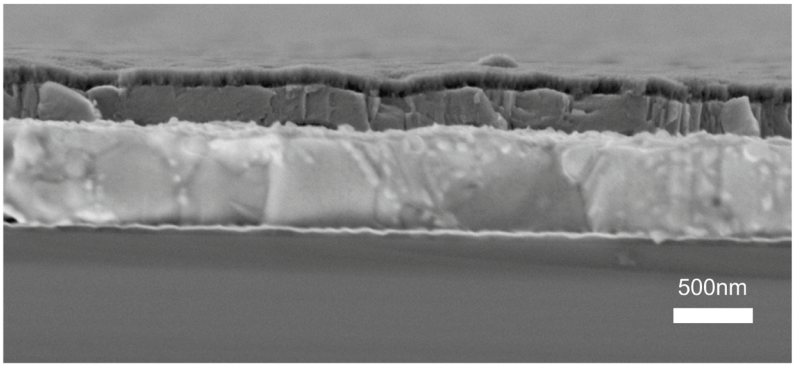

Figure S12. The cross-section SEM image of perovskite/Si tandem solar cell. White scale bar: 500nm.

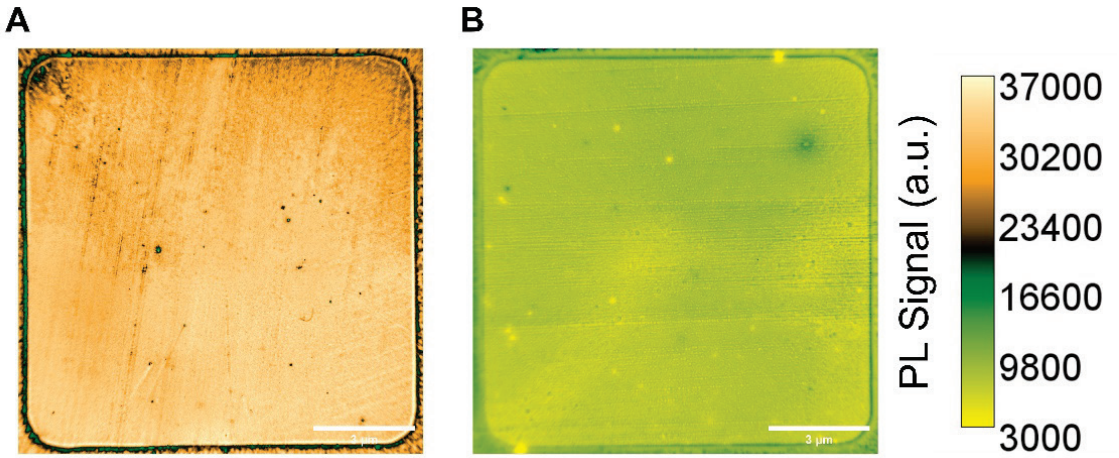

Figure S13. PL intensity maps of perovskite film performed on half stack samples (Si/ITO/NiO_X/2PACz/Perovskite/w.o. or w. Passivation) (A) passivated by $PDAI_2$/BAI with passivation layer and (B) without passivation layer. White scale bar: 3µm.

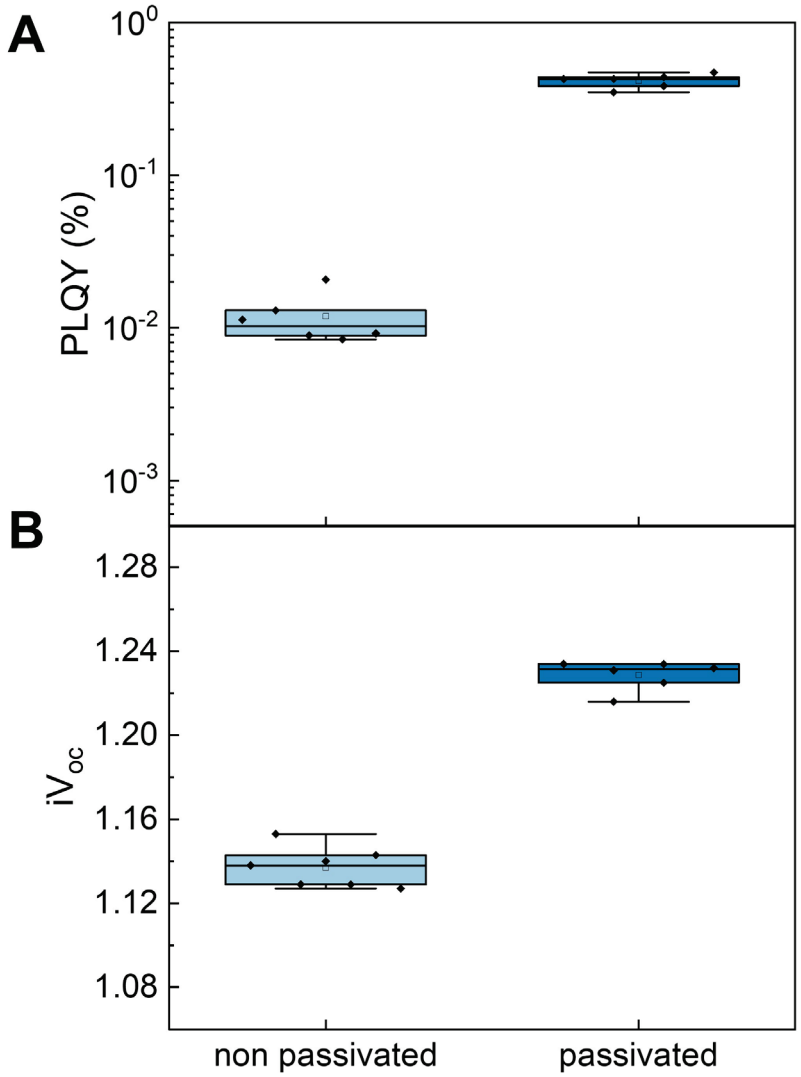

Figure S14. (A) PLQY and (B) iV_{oc} measurements of perovskite film performed on half stack samples (Si/ITO/NiO_X/2PACz/Perovskite/w.o. or w. Passivation)

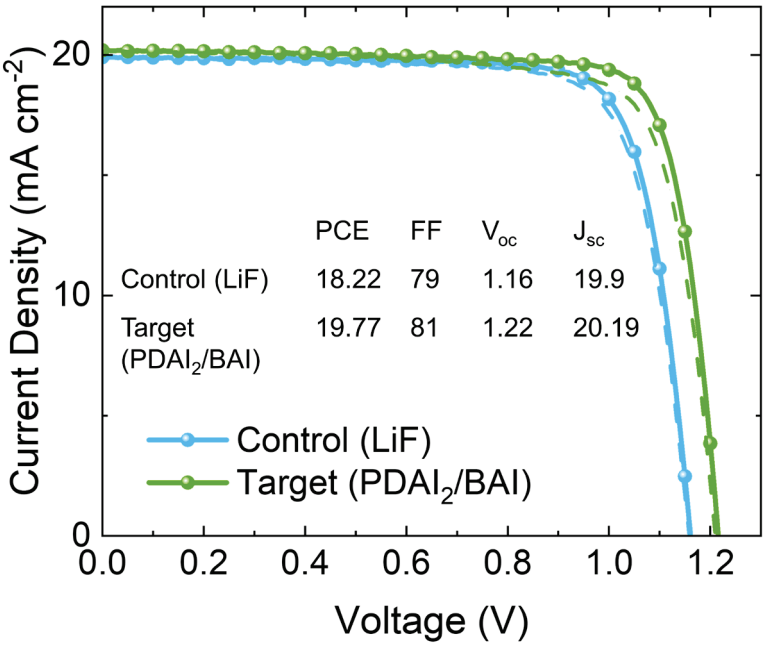

Figure S15. Comparison of *J-V* curves of single junction devices passivated by LiF (control) and $PDAI_2$/BAI (target).

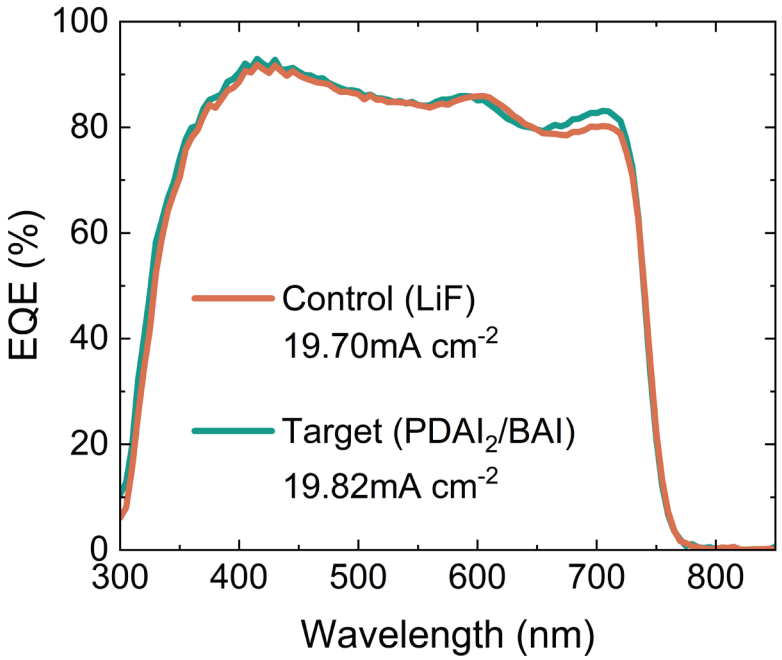

Figure S16. Comparison of EQE results of single junction devices passivated by LiF (control) and $PDAI_2$/BAI (target).

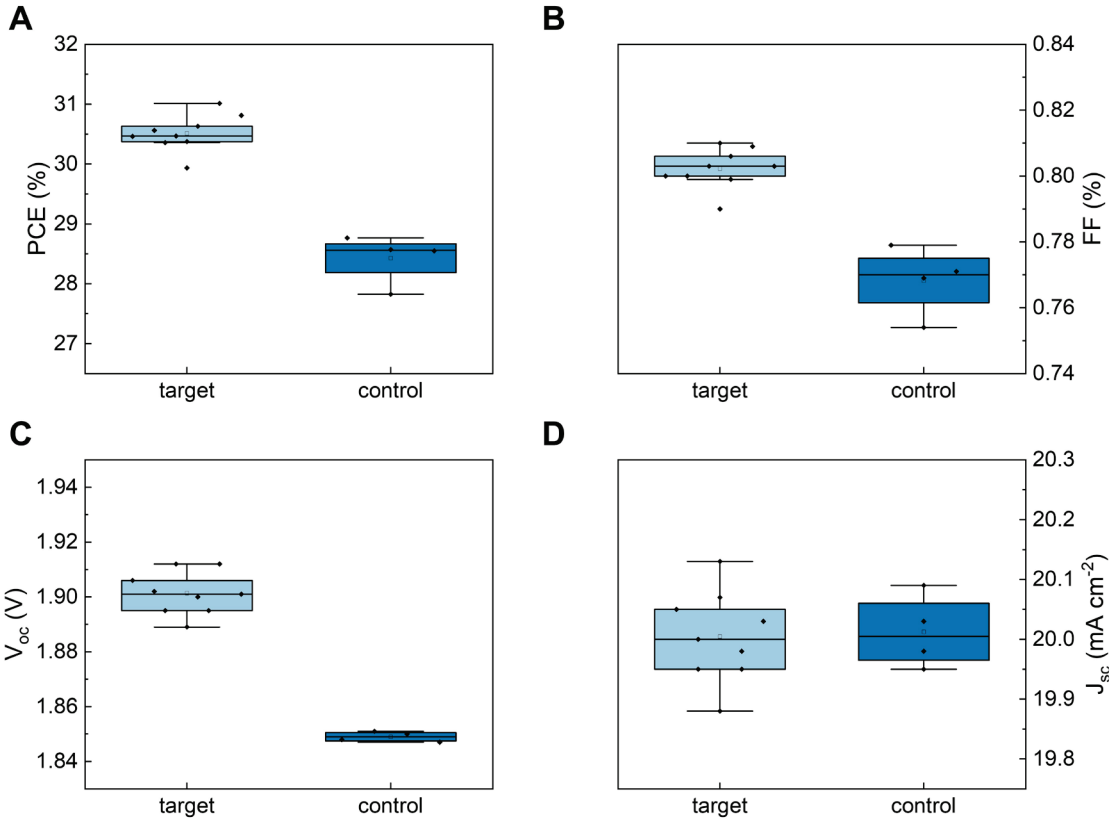

Figure S17. Statistical comparison of tandem cells performance passivated by LiF (control) and $PDAI_2$/BAI (target).

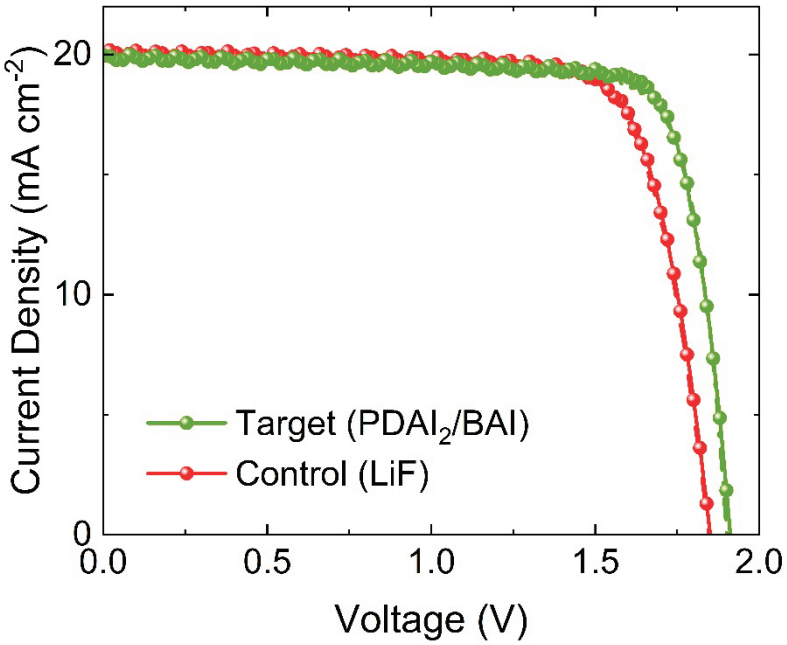

Figure S18. Comparison of *J-V* curves of perovskite/Si tandem devices passivated by 1nm LiF (control) and $PDAI_2$/BAI (target).

Reference

1. F. Haase, C. Hollemann, S. Schäfer, A. Merkle, M. Rienäcker, J. Krügener, R. Brendel and R. Peibst, *Solar Energy Materials and Solar Cells*, 2018, **186**, 184-193.
2. M. Rienäcker, M. Bossmeyer, A. Merkle, U. Römer, F. Haase, J. Krügener, R. Brendel and R. Peibst, *IEEE Journal of Photovoltaics*, 2016, **7**, 11-18.
3. R. Brendel and R. Peibst, *IEEE Journal of photovoltaics*, 2016, **6**, 1413-1420.
4. K. Ramspeck, S. Reißenweber, J. Schmidt, K. Bothe and R. Brendel, *Applied Physics Letters*, 2008, **93**.
5. Y. Yuan, G. Yan, C. Dreessen and T. Kirchartz, *Advanced Energy Materials*, 2024, 2403279.
6. J. C. de Mello, H. F. Wittmann and R. H. Friend, *Advanced materials*, 1997, **9**, 230-232.
7. M. Stolterfoht, M. Grischek, P. Caprioglio, C. M. Wolff, E. Gutierrez-Partida, F. Peña-Camargo, D. Rothhardt, S. Zhang, M. Raoufi and J. Wolansky, *Advanced Materials*, 2020, **32**, 2000080.
8. L. Krückemeier, U. Rau, M. Stolterfoht and T. Kirchartz, *Advanced energy materials*, 2020, **10**, 1902573.
9. Y. Wu, P. Zheng, J. Peng, M. Xu, Y. Chen, S. Surve, T. Lu, A. D. Bui, N. Li and W. Liang, *Advanced Energy Materials*, 2022, **12**, 2200821.
10. S. Jiang, Z. Ding, X. Li, L. Zhang, Z. Ying, X. Yang, Z. Yang, W. Yang, Y. Zeng and J. Ye, *Advanced Functional Materials*, 2024, **34**, 2401900.
11. B. Li, M. Härtel, A. Al-Ashouri, M. Simmonds, I. Taupitz, L. Kegelmann, E. Jarzembowski, F. Frühauf, E. Köhnen and L. Korte, *ACS Energy Letters*, 2024, **9**, 4550-4556.
12. Z. Ying, X. Yang, J. Zheng, J. Sun, J. Xiu, Y. Zhu, X. Wang, Y. Chen, X. Li and J. Sheng, *Solar RRL*, 2022, **6**, 2200793.
13. L. Qiao, T. Ye, T. Wang, W. Kong, R. Sun, L. Zhang, P. Wang, Z. Ge, Y. Peng and X. Zhang, *Advanced Energy Materials*, 2024, **14**, 2302983.
14. L. Wang, N. Wang, X. Wu, B. Liu, Q. Liu, B. Li, D. Zhang, N. Kalasariya, Y. Zhang and X. Yan, *Advanced Materials*, 2025, 2416150.
15. Z. Ding, C. Kan, S. Jiang, M. Zhang, H. Zhang, W. Liu, M. Liao, Z. Yang, P. Hang and Y. Zeng, *Nature Communications*, 2024, **15**, 8453.
16. Z. Ying, Z. Yang, J. Zheng, H. Wei, L. Chen, C. Xiao, J. Sun, C. Shou, G. Qin and J. Sheng, *Joule*, 2022, **6**, 2644-2661.
17. T. Han, W. Zhu, T. Wang, M. Yang, Y. Zhou, H. Xi, P. Zhong, D. Chen, J. Zhang and C. Zhang, *Advanced Functional Materials*, 2024, **34**, 2311679.
18. X. Guo, Z. Ying, X. Li, M. Zhang, S. Su, J. Zheng, H. Du, Y. Sun, J. Wu and L. Liu, *Advanced Energy Materials*, 2025, 2403021.
19. Z. Liu, Q. Han, Q. Wu, H. Du, M. Liao, W. Liu, Z. Yang, Y. Zeng and J. Ye, *Materials Today Energy*, 2024, **46**, 101721.
20. L. Duan, S. P. Phang, D. Yan, J. Stuckelberger, D. Walter, Y. Hou, W. Wang, N. Chang, A. D. Bui and A. O. Mayon, *Journal of Materials Chemistry A*, 2024, **12**, 20006-20016.
21. J. Zheng, Z. Ying, Z. Yang, Z. Lin, H. Wei, L. Chen, X. Yang, Y. Zeng, X. Li and J. Ye, *Nature Energy*, 2023, **8**, 1250-1261.